Numerical study of Strouhal instabilities in two-phase flows

M. Burger, R. Schmehl[1], O. Schäfer, R. Koch and S. Wittig

matthias.burger@its.uni-karlsruhe.de
Institut für Thermische Strömungsmaschinen, Universität Karlsruhe
76128 Karlsruhe, Germany
[1] Aerothermodynamics Section TOS-MPA/ESTEC, European Space Agency

Predicting fuel spray interaction with large scale vortex structures still is a major challenge for state-of-the-art flow predictions. In order to elucidate the mechanisms involved, a fundamental study has been carried out in which the interaction of water droplets with Strouhal instabilities is investigated. A disperse two-phase flow around a cylinder is computed taking into account heat and mass transfer for both phases. Flow conditions are chosen such that large scale vortices are generated by Strouhal instabilities of the well known Karman vortex street. A homogeneous distribution of water droplets is injected into hot air at the up-stream region of the computational domain. The mixing process as well as the impact of the droplets on the Strouhal instabilities is analyzed in the down-stream region with large scale vortex structures.

1 Introduction

In the present paper, the Strouhal instabilities of a Karman vortex street in the wake of a cylinder is considered and the two-phase flow of hot air seeded by water droplets is analyzed for laminar flow conditions. The statistical fluctuations of droplets in turbulent vortex structures is still a major challenge for state-of-the-art flow predictions. Many empirical droplet-turbulence interaction models have been published [8] [3] in which the dispersion models based on vortex time and length scales have been proposed. Only few publications address the direct numerical simulation of particle dispersion in large scale vortex structures [12].
The flow structures in the Karman vortex street have been studied in the context of Large Eddy Simulations [2] [11]. For single phase flows, the unsteady flow separation can be described by the Reynolds and Strouhal number [7] [9] [13]. However, in the case of a two-phase flow a more complex description is required [5].
The focus of the present paper is put on the effect of droplets on the flow structures in the Karman vortex street. In particular, the response of droplet to fluctuations of the gas flow is analyzed in terms of non-dimensional quantities. Using numerical predictions, the effect of droplet-loading and droplet size on the lift and drag coefficient of the cylinder is studied. The numerical part of the study is performed in three steps: First, only the vortex interaction between droplets and gas phase is studied, whereas the influence of the droplets on the gas phase is completely neglected. Then non-evaporating droplets are considered and momentum transfer between droplets and gas phase is taken into account. Finally, evaporating droplets are studied and all physical phenomena are included.

2 Theoretical analysis of particle motion in an oscillating gas phase

Particle motion in an unsteady flow can be described by the transfer function between gas and particle motion. In order to establish non-dimensional quantities describing this behavior, an analytical expression is derived for the particle motion in a gas flow field with sinusoidal velocity fluctuations.
Assuming a density ratio of $\rho_d/\rho_g \approx 10^3$, unsteady forces like the virtual mass effect and Basset force can be neglected. In this case, the equation of motion of a spherical particle in a gas flow is given by [5]

$$\frac{d\vec{u}_p}{dt} = -\frac{3}{4}\,\frac{\mu_g\, C_D\, Re_p}{D_p^2}(\vec{u}_p\,-\,\vec{u}_g)\,, \quad Re_p\,=\,\frac{\rho_g\, D_p}{\mu_g}\,|\vec{u}_p\,-\,\vec{u}_g|\,. \tag{1}$$

Equation 1 can be linearized for Stokes flow conditions ($Re_p < 1$), i.e. by setting the drag coefficient $C_D = 24/Re_p$. This assumption is true for small particles and a moderate relative velocity $|\vec{u}_p - \vec{u}_g|$. Under these conditions, the particle motion is described by

$$\frac{d\vec{u}_p}{dt} = -\frac{1}{\tau}\,(\vec{u}_p\,-\,\vec{u}_g)\,, \quad \tau\,=\,\frac{\rho_d\, D_p^2}{18\,\mu_g}\,. \tag{2}$$

In order to study the response function of a particle in an oscillating gas flow field, the gas velocity u_g in Eq. 2 is replaced by a sinusoidal function $u_g = u_{g,0} + \hat{u}\ sin(\omega t)$. As a steady velocity has no effect on the particle oscillation, $u_{g,0}$ is set to zero in this study. The solution of this equation for the initial condition of the particle velocity $u_{p,0} = 0$ is given by

$$u_p\,=\,\underbrace{\frac{\tau\omega\,\hat{u}}{1+\tau^2\omega^2}exp\left(-\frac{t}{\tau}\right)}_{initial\ noise} + \underbrace{\underbrace{\frac{\hat{u}}{\sqrt{1+\tau^2\omega^2}}}_{amplitude}\,sin\left(\omega t + \underbrace{\arctan(\tau\omega)}_{phase\ shift}\right)}_{oscillation}\,. \tag{3}$$

Equation 3 reveals that the particle motion is governed by two terms: a decaying initial noise and the oscillation of the particle. The oscillation is characterized by the phase shift and the amplitude term. As the discrepancy between particle motion and gas motion is of major interest in this study, the amplitude difference will be used instead of the amplitude subsequently.
In general, two-phase flows are characterized by the Stokes number [5]. The Stokes number of a particle in a harmonically oscillating gas flow is given by $St = \tau\omega/2\pi$. It represents the non-dimensional time scale ratio of particle motion and gas flow oscillation $St = \tilde{t}_p/\tilde{t}_g$. The Stokes number is well-suited to quantify the particle dynamics. The noise factor N and the amplitude difference factor ΔA as well as the phase shift factor P of Eq. 3 can be written as non-dimensional quantities in terms of the Stokes number St:

$$N\,=\,\frac{2\pi St}{1+(2\pi\cdot St)^2}\cdot exp\left(-\frac{1}{St}\right)\,,\ \Delta A\,=\,1-\frac{1}{\sqrt{1+(2\pi\cdot St)^2}}\,,\ P\,=\,\frac{2}{\pi}\cdot\arctan(2\pi\cdot St)\,. \tag{4}$$

These quantities describe the discrepancy of particle response to the gas fluctuation as a function of the Stokes number. In the limiting case of $St \to 0$, all numbers approach zero, i.e. the particle reproduces exactly the gas velocity. For $St \to \infty$ the gas velocity does not effect the particle. The noise factor N, the amplitude difference factor ΔA and the phase shift factor P as a function of St are illustrated in Fig 1. The noise factor N reaches its maximum at a Stokes

number of one. A phase shift is present even for small Stokes numbers, whereas the amplitude difference and the noise are important if the Stokes number is larger by at least one order of magnitude. If $St \leq 0.002$, all numbers are less than 0.01. In this case, the particle-air mixture can be regarded as a single phase fluid with modified properties (e.g. density).

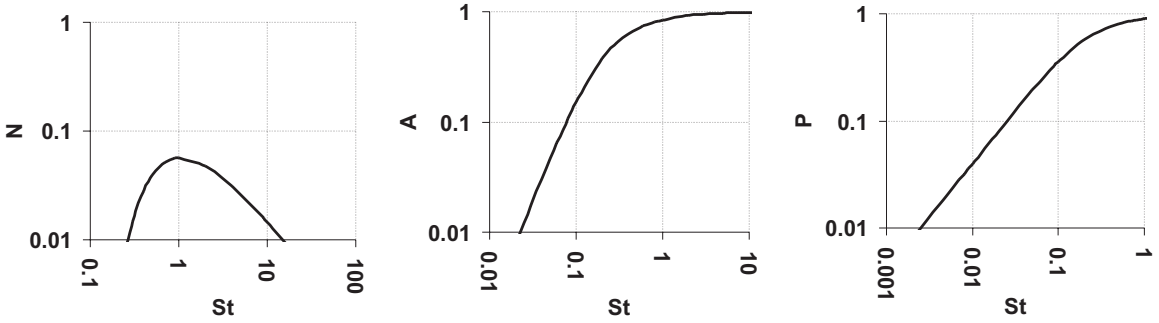

Figure 1: Noise factor N [left], amplitude difference factor ΔA [center] and phase shift factor P [right]

An analytical expression of the particle displacement can be derived by integration of Eq. 3. Assuming an initial particle starting condition $x_{p,t=0} = 0$, the particle displacement is given by

$$x_p = \underbrace{\frac{\hat{u}}{\omega}}_{mean} - \underbrace{\frac{\hat{u}}{\omega}\frac{\tau^2\omega^2}{1+\tau^2\omega^2} exp\left(-\frac{t}{\tau}\right)}_{initial\ noise} - \underbrace{\frac{\hat{u}}{\omega}\frac{1}{\sqrt{1+\tau^2\omega^2}}}_{amplitude} cos\left(\omega t - \underbrace{\arctan(\tau\omega)}_{phase\ shift}\right) . \quad (5)$$

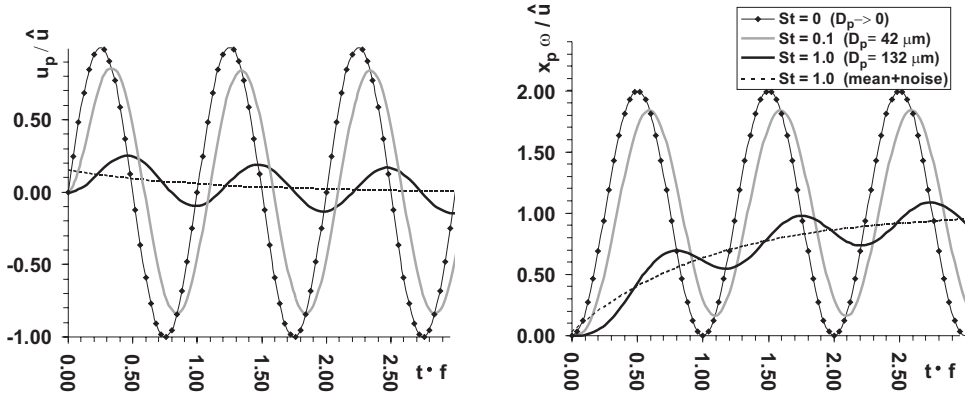

Figure 2: Response function of a water droplet in an oscillating air flow field ($f = 20\ Hz$) for different Stokes numbers at standard conditions: Normalized droplet velocity (Eq. 3) [left] and droplet displacement (Eq. 5) [right]

Comparing particle displacement (Eq. 5) and particle velocity (Eq. 3) the normalized terms for amplitude and phase shift are identical, only the noise term is different. The mean value of the particle displacement is $x_p = \hat{u}/\omega$. This term indicates that a particle which was started at $x_{p,t=0} = 0$ tends to approach an asymptotic displacement for $t \rightarrow \infty$ which is identical to the mean displacement of the gas phase. This process can be observed in Fig. 2 in which the velocity and displacement of a water droplet in an oscillating gas flow field is illustrated for standard conditions.

3 Prediction of the Karman vortex street in the wake of an annular cylinder

In the present study the Karman vortex street was analyzed for a disperse two-phase flow at laminar flow conditions. Hot air ($T_{g,0} = 373\ K$) enters the computational domain at the up-stream boundary. A homogeneous distribution of mono disperse water droplets ($T_{d,0} = 293\ K$) is injected at a cross-section 16.25 mm up-stream of the cylinder. The inlet velocity ($u_0 = 0.3166\ \frac{m}{s}$) is identical for both phases and chosen such that the Reynolds number of the air flow is $Re = 100$. The cylinder has a diameter of $D_{cyl} = 7.5\ mm$ and a constant temperature of $T_{cyl} = 373\ K$. No slip conditions are assumed at the surface of the cylinder. The dimension of the domain is chosen such that the symmetry and outlet boundaries have no effect on the vortex street. The computational domain is depicted in Fig. 3. The overall grid size is 10,170 cells.

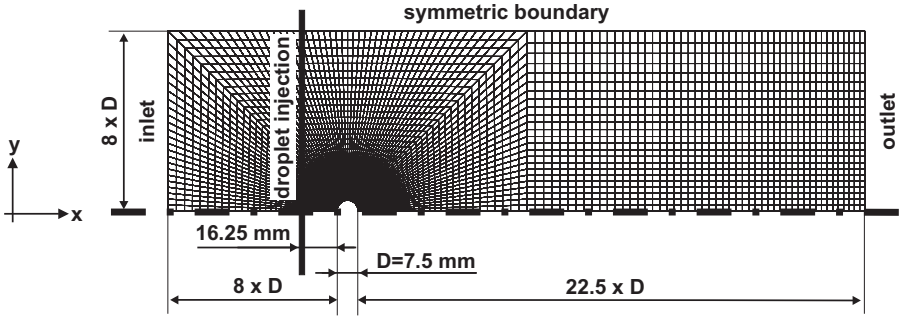

Figure 3: Computational domain

3.1 Numerical methods

The gas flow is predicted by a Navier-Stokes equation based Finite-Volume method. For discretization in space and time, the Monotonized Linear Upwind scheme [10] and the time-implicit three level scheme [6] are used in the present study. Both methods are of second order accuracy. The droplet phase is predicted by a Lagrangian method in which a statistically sufficient number of trajectories is counted. Droplet evaporation is taken into account by the Uniform Temperature Model [1] and the interaction of the two phases is considered by exchanging source terms for mass, momentum and energy between the Navier-Stokes and the Lagrangian code. In order to comply within CFL condition ≤ 1, a time step of 1 ms ($\omega t \leq 0.05$) was chosen for the computation of both phases. The comprehensive description of the numerical procedure was already published [4].

3.2 Single phase flow

The periodic flow separation in the wake of the cylinder produces nearly sinusoidal pressure and velocity fluctuations. Pressure and shear stress forces on the cylinder are also characterized by these fluctuations. This process can by studied by mapping the time-dependent drag and lift coefficients C_D and C_L of the cylinder. The definition of these integral quantities is given by

$$C_D = \frac{\int_A F_x dA}{\frac{1}{2}\rho U_0^2 D_{cyl}\, H_{cyl}}\ , \quad C_L = \frac{\int_A F_y dA}{\frac{1}{2}\rho U_0^2 D_{cyl}\, H_{cyl}}\ , \quad \vec{F} = \underbrace{\int_A p\,\vec{n}\,dA}_{pressure\ force} + \underbrace{\int_A \vec{\tau}\,dA}_{shear\ stress\ force} \quad . \tag{6}$$

The predicted results of the Karman vortex street for pure air flow are illustrated in Fig. 4. In the left plot the pressure fluctuation around the cylinder is depicted, in the right plot the drag and lift coefficient as well as the pressure and shear stress components are shown.
Strouhal studied the frequencies of this instability for different Reynolds numbers and derived the non-dimensional Strouhal number $Str = (D_{cyl}/u_0) \cdot f$ [7]. The Strouhal number of the present flow is 0.172. This value agrees with experimental results indicating a Strouhal number of Str = 0.152-0.173 [9] and Str = 0.164 [13]. The computed results of the lift coefficient (Fig. 4) reproduce exactly the Strouhal frequency, whereas the drag coefficient oscillates with the double frequency.

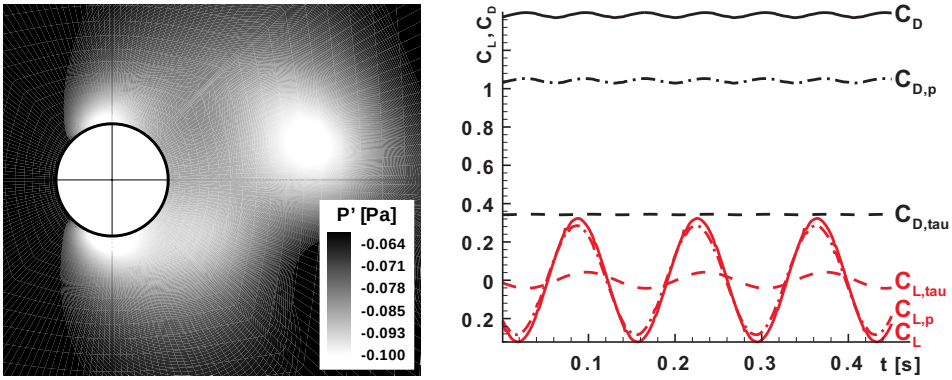

Figure 4: Normalized pressure distribution of the Karman vortex street (Re=100) in a pure air flow ($T_g = 373\ K$) [left], drag and lift coefficient of the annular cylinder [right]

3.3 Droplet dispersion in the Karman vortex street (one-way coupled)

The distribution of the disperse phase in the wake of the cylinder is strongly affected by vortex-particle interaction. In order to study the interaction, droplets are not injected in the whole cross-section up-stream of the cylinder as described in section 3. They are only injected in the projection area of the cylinders cross-section (Fig. 5). In order to study the droplet motion separately, the droplet-loading $z = \dot{m}_d/\dot{m}_g$ is set to zero and droplet evaporation is neglected. Thus, no exchange of source terms occurs throughout the prediction (one-way coupled). The impact of gas fluctuations on droplet motion depends strongly on the droplet size. The results for different droplet diameters are depicted in Fig. 5.
The predicted droplet distributions show that small droplets with a diameter of $D_d = 10\ \mu m$ ($St = 0.002$) instantly follow the gas flow and exactly trace the vortex structures. Spray separation can be observed for larger droplet diameters ($D_d = 30,\ 50\ \mu m$) resulting in an accumulation of droplets at the peripheries of the vortex structures. In the case of 100 μm droplets, the vortex street can not be reproduced.
In general, droplets characterized by $St \leq 0.002$ behave like a passive scalar with no diffusion. At higher Stokes numbers, droplets are separated and accumulated at the peripheries. If the Stokes number is larger by orders of magnitude, the particles do not follow the flow in vortex structures. This phenomenon can be explained by the phase shift factor P (Fig. 1). For 100 μm droplets, the phase shift factor is $P = 0.57$ indicating that the particles follow the gas flow with a time-lag of $0.57 \cdot T$ which is more than half of the cycle duration T. Despite identical unsteady structures of the gas phase, the droplet trajectories are deflected significantly and the pattern of the droplet motion deviates from that of the gaseous phase.

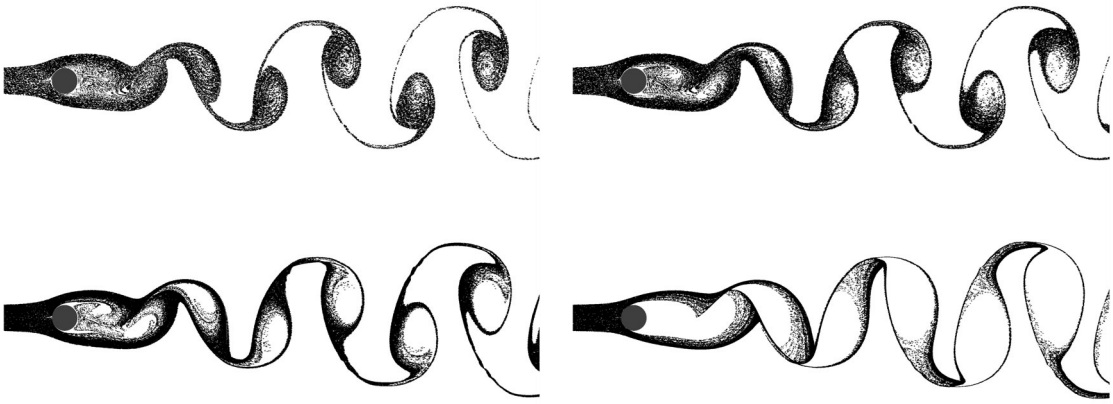

Figure 5: Instantaneous droplet distribution in the Karman vortex street ($Re = 100,\ f \approx 7{,}3\ Hz$): $D_d = 10\ \mu m$ (St=0.002) [top left], $D_d = 30\ \mu m$ (St=0.02) [top right], $D_d = 50\ \mu m$ (St=0.05) [bottom left] and $D_d = 100\ \mu m$ (St=0.2) [bottom right]

3.4 Analysis of a non evaporating droplet-air mixture (two-way coupled)

The emphasis in this section is put on the two-way coupled prediction of the Karman vortex street. Whereas the influence of the disperse phase on the flow field can be neglected for $z \rightarrow 0$, a decisive influence is observed for $z > 0$. The vortex structures of the gas phase are affected by the presence of the spray. This effect is taken into account by exchanging source terms of the disperse phase (two-way coupling). In a first step this phenomenon is analyzed for a non-evaporating spray. This way, the gas phase is only affected by the momentum source terms of the spray.

Effect of the droplet-loading

A parametric study has been carried out with objective to identify the effect of droplet-loading z on the gas flow. The droplet diameter is kept constant. For reproducing a Stokes number St = 0.002, a droplet diameter $D_d = 10\ \mu m$ is chosen for this analysis. Under these conditions, the theoretical study of section 2 revealed that the two-phase flow can be regarded as a single continuum with a modified density $\rho_m = (1+z)\rho_g$ [5]. The Reynolds number of the two-phase mixture is given by $Re_m = (1+z)Re_g$. As the instabilities depend on the Reynolds number, the vortex street is affected by the droplet-loading z. In order to quantify this phenomena, the drag and the lift coefficient are evaluated in the range $Re = 100 - 120$. The predicted results are depicted in Fig. 6. In order to support the theoretical findings from section 2, the two-phase calculations are compared to computational predictions and experiments [9] of single phase flows. Obviously, the drag and lift coefficients of the two-phase flow agree well with the single phase results.

Variation of the droplet diameter

The response function of particle motion was shown to be almost identical to the motion of the gas phase (deviation < 1%) for $St \leq 0.002$. However, at higher Stokes numbers the phase shift and the amplitude difference increase dramatically. As consequence, the particle motion strongly deviates from the motion of the gas phase. In this case, the two-phase mixture can not be regarded as a single phase flow. In order to quantify this effect, the Karman vortex street in the two-phase mixture is predicted for varying droplet diameters in the range $D_d = 1 - 50\ \mu m$

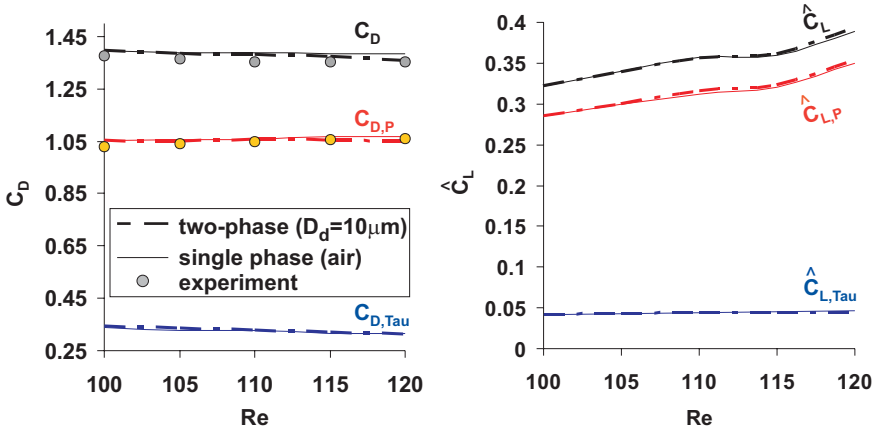

Figure 6: Drag coefficient C_D [left] and max. lift coefficient $\hat{C}_L$ [right] for varying droplet-loadings $z = 0.0 - 0.2$ ($Re_m = 100 \ldots 120$) and a constant droplet diameter $D_d = 10\ \mu m$ ($St = 0.002$) compared to single phase predictions and experiments [9]

(St= 2.0E-5 - 0.05), whereas the droplet-loading $z = 0.1$ is kept constant. The predictions of the drag and lift coefficient of the cylinder are illustrated in Fig. 7. Obviously, the drag coefficient of the cylinder is not affected by droplets being more or less accumulated at the periphery of the eddies in the wake of the cylinder. In contrast, the lift coefficient clearly depends on the size of the droplets. As illustrated in Fig. 5, a max. lift coefficient of $\hat{C}_L = 0.355$ is predicted for a droplet diameter $D_d \leq 10\ \mu m$. This result reflects the previous finding that the two-phase mixture containing only small droplets is comparable to a single phase flow. For bigger droplets the lift coefficient decreases strongly. An abrupt decrease is found at a droplet diameter of $D_d \approx 10\ \mu m$ ($St = 0.002$) and $D_d \approx 30\ \mu m$ ($St = 0.02$). This phenomenon can be explained by considering the phase shift factor P and amplitude difference factor ΔA as derived in section 2. It was shown in Fig. 1, that the phase shift factor P strongly increases at a Stokes number of $St = 0.002$ and the amplitude difference factor ΔA at $St = 0.02$. The rise of both factors is reflected in a sudden decrease of the lift coeffcient. However, the study indicates that the amplitude difference has a much stronger impact on C_L than the phase shift. Thus, the theoretical analysis of section 2 is confirmed by the numerical predictions of this test case.

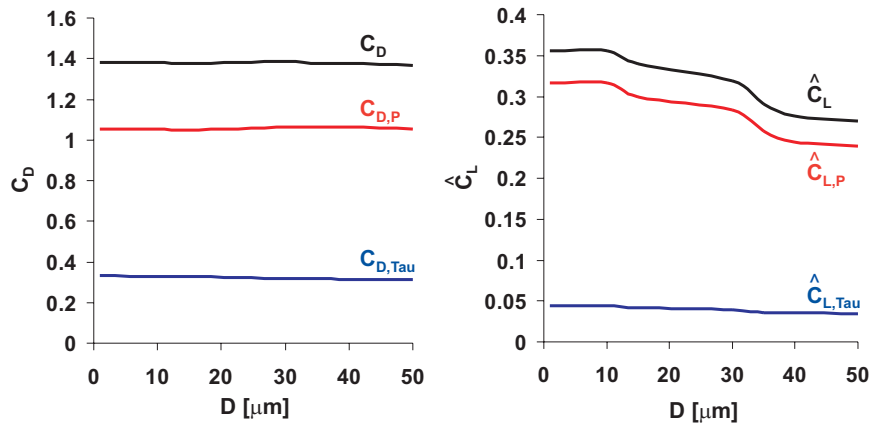

Figure 7: Drag coefficient C_D [left] and max. lift coefficient $\hat{C}_L$ [right] for varying droplet sizes $D_d = 1 - 50\ \mu m$ and a constant particle-loading $z = 0.1$

3.5 Analysis of an evaporating droplet-air mixture (two-way coupled)

The focus of this last section is placed on an evaporating droplet air mixture exposed to heat and mass transfer of both phases. The interaction between the disperse phase and the gas phase is considered by source term coupling. The simulations are carried out for a mono disperse water spray ($D_{d,0} = 30\ \mu m,\ T_{d,0} = 293\ K,\ z = 0.025$) in hot air ($T_{g,0} = 373\ K$). The results in terms of vapor mass fraction and gas temperatures are illustrated in Fig. 8. In contrast to a non evaporating spray, the vortex street is significantly affected by the spray despite the low droplet-loading z. Due to droplet evaporation, the gas flow is characterized by intense local temperature drops which in turn affect the fluid properties. Droplets are instantly evaporated in the vicinity of the hot cylinder surface ($T_{cyl} = 373\ K$) resulting in an inhomogeneous distribution of vapor concentration, gas temperature and droplets in the downstream region.

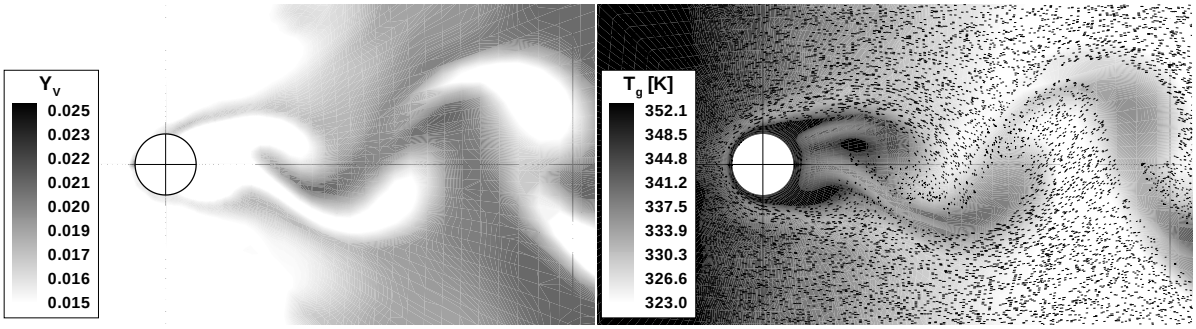

Figure 8: Predicted results of the Karman vortex street of an evaporating flow of hot air ($T_{g,0} = 373\ K$) and a mono disperse water spray ($D_{d,0} = 30\ \mu m,\ T_{d,0} = 293\ K,\ z = 0.025$): vapor mass fraction Y_v [left], gas temperature T_g and droplets [right]

4 Conclusion

In the present paper the Karman vortex street of a two-phase flow was analyzed for laminar flow conditions. A theoretical analysis of the governing equations revealed that the response of the droplet to the harmonically oscillating flow field can be described by an initial noise term and a droplet oscillation term. Both, the amplitude and the phase shift of the droplet oscillation term are a function of the Stokes number. Most importantly, it was shown that the capability of droplets to follow the oscillations of the gas flow field is reduced by an increasing Stokes number.

These theoretical findings were confirmed by the numerical prediction of the two-phase flow in a Karman vortex street. Depending on the Stokes number the particles are accumulated in the periphery of the wake of the Karman vortex street. At a higher Stokes number of $St = 0.2$ the pattern of the droplet motion deviates strongly from that of the gaseous phase.

The influence of the droplet-loading was studied and it was found that the vortex street is changed by the presence of the spray. The prediction revealed, that for small Stokes numbers ($St \leq 0.002$) the two-phase flow can be treated like a single phase with a modified density. The Stokes number was found to significantly affect the lift coefficient of the cylinder. In particular, step-like changes were identified at $St \approx 0.002$ and $St \approx 0.02$.

5 Acknowledgement

This work was partly supported by the German Science Foundation in the framework of the Sonderforschungsbereich 606 which is gratefully acknowledged. The authors would like to thank Mr. C. Klostermeier for his valuable contribution to this project.

References

[1] B. Abramzon and W. A. Sirignano. Droplet Vaporisation Models for Spray Combustion Calculations. *International Journal of Heat and Mass Transfer*, 32:1605–1618, 1989.

[2] P. Beaudan and P. Moin. Numerical experiments on the flow past a circular cylinder at sub-critical Reynolds number. Technical Report TF-62, Stanford University, Thermoscience Division, Department of Mechanical Engineering, 1994.

[3] E. Blümke. Turbulente Partikeldispersion in eingeschlossenen Drallströmungen. Dissertation, Ruhr-Universität Bochum, Köln, 1992.

[4] M. Burger, R. Schmehl, K. Dullenkopf, O. Schäfer, R. Koch, and S. Wittig. Predictions of Transient Fuel Spray Phenomena in the Intake Port of a SI-Engine. *SAE Tech. Paper, Nr. 2002-01-2695, San Diego*, 2002.

[5] C. Crowe, M. Sommerfeld, and Y. Tsuji. *Multiphase Flows with Droplets and Particles*. CRC Press, 1 edition, 1998.

[6] J. H. Ferzinger and M. Perić. *Computational Methods for Fluid Dynamics*. Springer-Verlag, 1996.

[7] S. I. Green. *Fluid Vortices*. Kluwer Academic Publishers, 1995.

[8] G. Klose, B. Rembold, R. Koch, and S. Wittig. Comparison of state of the art droplet-turbulence models for aero-engine combustor conditions. In *3rd International Symposium on Turbulence, Heat and Mass Transfer, in Nagoya, Japan*, April 2-6, 2000.

[9] J.H. Lienhard. Synopsis of lift, drag and vortex frequency for riged circular cylinders. College of Engineering Research Division bulletin 300, Techn. Extension Service, Washington State University, 1966.

[10] B. Noll. Evaluation of a High-Resolution Scheme for Combustor Flow Computations. *AIAA-Journal*, 30(1):64–69, 1992.

[11] Wolfgang Rodi. Large-eddy simulations of the flow past bluff bodies: State-of-the-art. *JSME International Journal, Series B*, 41(2):361–374, 1998.

[12] L. Tang, F. Wen, Y. Yang, C.T. Crowe, J.N. Chung, and T.R. Troutt. Self-organizing particle dispersion mechanism in free shear flows. *Physics of Fluids A*, 4:2244, 1992.

[13] C.H.K. Williamson. Defining a universal and continuous strouhal-reynolds number relationship for the laminar vortex shedding of a cicular cylinder. *Physics of Fluids*, 31(10): 2742–2744, 1988.